Optimizing nonlinear beam coupling in low-symmetry crystals

A. Shumelyuk,[1,*] A. Volkov,[1] S. Odoulov,[1] A. Grabar,[2] I. Stoyka,[2] and D. R. Evans[3]

[1] *Institute of Physics, National Academy of Sciences, 46, Science Avenue, 03 650 Kyiv, Ukraine*
[2] *Uzhgorod National University, Uzhgorod, Ukraine*
[3] *Air Force Research Laboratory, Materials and Manufacturing Directorate, WPAFB, OH, 45433, USA*
[*] *shumeluk@iop.kiev.ua*

Abstract: The purpose of this paper is to find the polarizations and spatial orientations of the two interacting counterpropagating coherent light waves which ensure the largest beam coupling in monoclinic photorefractive crystal. The results of calculations are presented that are verified experimentally with $Sn_2P_2S_6$.

OCIS codes: (160.5320) Photorefractive materials; (190.5330) Photorefractive nonlinear optics; (300.6420) Spectroscopy, nonlinear.

References and links

1. A. A. Grabar, M. Jazbinšek, A. N. Shumelyuk, Yu. M. Vysochanskii, G. Montemezzani, and P. Günter, "Photorefractive effects in $Sn_2P_2S_6$," in *Photorefractive Materials and Their Applications II*, P. Günter and J.-P. Huignard, eds. (Springer Verlag, 2007).
2. Y. Petit, S. Joly, P. Segonds, and B. Boulanger, "Recent advances in monoclinic crystal optics," Laser Photon. Rev. **7**(6), 920–937 (2013).
3. A. Shumelyuk, S. Odoulov, G. Cook, and D. R. Evans, "Coupling of counterpropagating light beams in low symmetry photorefractive crystals," Opt. Lett. **34**(14), 2126–2128 (2009).
4. A. Shumelyuk, A. Volkov, S. Odoulov, G. Cook, and D. R. Evans, "Coupling of counterpropagating light waves in low-symmetry photorefractive crystals," Appl. Phys. B **100**(1), 101–108 (2010).
5. X. Yue, F. Mersch, R. Rupp, U. Hellwig, and M. Simon, "Holographic recording and beam coupling in ferroelectric $Bi_4Ti_3O_{12}$," Phys. Rev. B **53**, 8967–8970 (1996).
6. X. Yue, J. Xu, F. Mersch, R. A. Rupp, and E. Krätzig, "Photorefractive properties of $Bi_4Ti_3O_{12}$," Phys. Rev. B **53**, 9495–9502 (1997).
7. G. Montemezzani, J. Fousek, P. Günter, and J. Stankowska, "Phase gratings in Fe^{3+}-doped triglycine sulphate single crystals recorded in the ultraviolet spectral region," Appl. Phys. Lett. **56**, 2367–2369 (1990).
8. G. Montemezzani and M. Zgonik, "Light diffraction at mixed phase and absorption gratings in anisotropic media for arbitrary geometries," Phys. Rev. E **55**(1), 1035–1047 (1997).
9. Y. M. Vysochanskii and V. Y. Slivka, "Ferroelectrics of the $Sn_2P_2S_6$ family. Properties in Vicinity of Lifshitz Point" (Oriana-Nova, 1994) (in Russian).
10. V. M. Kedyulich, A. G. Slivka, E. I. Gerzanich, P. P. Guranich, V. S. Shusta, and P. M. Lucach, "The influence of the temperature and uniform pressure on the anisotropy of dielectric properties of the $Sn_2P_2S_6$ crystal," Uzhgorod Univ. Bull. Phys. Ser. **5**, 30–32 (1999).
11. A. Shumelyuk, D. Barilov, S. Odoulov, and E. Krätzig, "Anisotropy of the dielectric permittivity of $Sn_2P_2S_6$ measured with light-induced grating techniques," Appl. Phys. B **76**(4), 417–421 (2003).
12. D. Haertle, A. Guarino, J. Hajfler, G. Montemezzani, and P. Günter, "Refractive indices of $Sn_2P_2S_6$ at visible and infrared wavelengths," Opt. Express **13**(6), 2046–2057 (2005).
13. C. Traum, P. L. Inácio, C. Félix, P. Segonds, A. Peña, J. Debray, B. Boulanger, Y. Petit, D. Rytz, G. Montemezzani, P. Goldner, and A. Ferrie, "Direct measurement of the dielectric frame rotation of monoclinic crystals as a function of the wavelength," Opt. Mater. Express **4**, 57–62 (2014).

#217677 - $15.00 USD Received 23 Jul 2014; revised 22 Sep 2014; accepted 22 Sep 2014; published 2 Oct 2014

14. D. Haertle, G. Caimi, A. Haldi, G. Montemezzani, P. Günter, A. A. Grabar, I. M. Stoika, and Yu. M. Vysochanskii, "Electro-optical properties of $Sn_2P_2S_6$," Opt. Commun. **215**(4), 333–343 (2003).
15. A. Volkov, A. Shumelyuk, S. Odoulov, D. R. Evans, and G. Cook, "Anisotropic diffraction from photorefractive gratings and Pockels tensor of $Sn_2P_2S_6$," Opt. Express **16**(21), 16923–16934 (2008).
16. G. Montemezzani, M. Aillerie, X. Zheng, H. Remmach, and A. Grabar, "Third column electro-optical coefficients of monoclinic $Sn_2P_2S_6$," Opt. Mater. Express **2**(7), 920–928 (2012).
17. A. Volkov, "Evaluation of non-diagonal components of Pockels tensor for photorefractive $Sn_2P_2S_6$ crystal," Ukr. J. Phys. **58**(4), 335–340 (2013).
18. A. Grabar, "Energy spectra and photoinduced phenomena in ferroelectrc-semiconductor of $Sn_2P_2S_6$ family," Dr of Science Thesis, Uzhgorod National University, Ukraine, Uzhgorod (2004).
19. D. Haertle, "Photorefractive and nonlinear properties of $Sn_2P_2S_6$," PhD Thesis, ETH No. 16107, Zürich (2005).
20. G. Dittmar and H. Schäfer, "Die Stuktur des Di-Zinn-Hexathiohypodiphoshatus $Sn_2P_2S_6$," Z. Naturforsch. **29B**(5–6), 312–317 (1974).
21. ANSI/IEEE, Std 176 - IEEE Standard on Piezoelectricity (IEEE, 1987), p. 242.
22. C. D. Carpentier and R. Nitsche, "Ferroelectricity in $Sn_2P_2S_6$," Mater. Res. Bull. **9**(8), 1097–1100 (1974).
23. M. M. Major, Yu. M. Vysochanskii, I. P. Prits, Sh. B. Molnar, V. Yu. Slivka, E. D. Rogach, F. I. Savenko, and A. P. Kudinov, "Piezoeffect in $Sn_2P_2S_6$ single crystals," Bull. USSR Acad. Sci., Inorg. Mater. **27**(3), 604–606 (1991).
24. T. Bach, M. Jazbinšek, G. Montemezzani, P. Günter, A. Grabar, and Yu. Vysochanskii, "Tailoring of infrared photorefractive properties of $Sn_2P_2S_6$ crystals by Te and Sb doping," J. Opt. Soc. Am. B **24**(7), 1535–1541 (2007).
25. A. Shumelyuk, A. Volkov, A. Selinger, M. Imlau, and S. Odoulov, "Frequency-degenerate nonlinear light scattering in low-symmetry crystals," Opt. Lett. **33**(2), 150–152 (2008).

1. Introduction

Finding conditions that ensure the largest nonlinear beam coupling is not a trivial problem in low symmetry crystals (triclinic or monoclinic) because of several reasons. First, the number of nonvanishing components of the Pockels tensor r_{ij} is at least doubled comparing to classical tetragonal photorefractive $BaTiO_3$. Second, in crystals with limited trap density the anisotropy of low-frequency dielectric permittivity ε_{kl} becomes important for estimating space charge screening effects. Third, in crystals of *m* symmetry class which are of special interest because of practical importance of photorefractive tin hypothiodiphosphate $Sn_2P_2S_6$ (SPS) [1], the frames for various anisotropic physical properties (for example, for low-frequency dielectric permittivity, index of refraction (optical indicatrix), linear and nonlinear absorption, fluorescence, etc.) do not coincide with the crystallographic frame (see, for example recent review article [2]).

Previous attempts to optimize the orientation of the space charge grating and the recording waves polarization in $Sn_2P_2S_6$ in order to get the largest possible nonlinear coupling are described in Refs. [3, 4]. It has been shown that for interaction of counterpropagating waves the two beam coupling gain can be enhanced 1.5 times if the space charge grating is tilted roughly to 70° in the *xy* crystallographic plane with respect to standard orientation of the grating vector **K** along the *x*-axis.

In this paper it is shown that for the interaction of He-Ne laser light waves (633 nm) at room temperature the grating vector directions **K** for which the gain factor Γ takes its largest possible value do not appear in any of three standard crystallographic planes of $Sn_2P_2S_6$. This largest gain factor can be achieved for crystal eigenwave that corresponds to the inner shell of the normal surface in the wavevector space. The mirror plane (010), which is the only symmetry element of $Sn_2P_2S_6$ at ambient conditions imposes, in this case, the existence of two equivalent **K** directions that optimize beam coupling. For the eigenwave which corresponds to the outer shell there exists, however, only one optimum direction that maximizes beam coupling, because it is located in the mirror plane itself. In the latter case the largest gain factor peaks at about 0.7 of the possible absolute maximum value.

We present below the results of calculations (Sect. 2) that are further confirmed experimen-

#217677 - $15.00 USD Received 23 Jul 2014; revised 22 Sep 2014; accepted 22 Sep 2014; published 2 Oct 2014

tally by measurements with special cut $Sn_2P_2S_6$ samples (Sect. 3). An essential part of this paper describes our efforts to summarize data on $Sn_2P_2S_6$ characterization from different literature sources and present them within the same coordinate system to perform correct calculations. The Appendix describes how one can find experimentally the positive directions of coordinate axes for the accepted convention. The methods are discussed on how to establish the orientation of the optical indicatrix and spontaneous polarization $\mathbf{P}_S$ direction from their photorefractive manifestations.

The above analysis might be of importance for studies of other anisotropic properties of $Sn_2P_2S_6$ crystals. With any modifications it can be used for characterization of photorefractive $Bi_4Ti_3O_{12}$ that belongs to the same symmetry group as $Sn_2P_2S_6$ [5,6]. The proposed approach will be useful also for studies of index gratings in other low symmetry materials (see, e.g., Ref. [7]).

2. Calculations of gain factor for different orientations of two counterpropagating waves

The general expression for two-beam coupling gain in a crystal with diffusion driven charge transport (see, e.g., Ref. [8]) is as follows:

$$\Gamma = (\mathbf{e}_s \cdot \mathbf{e}_p) \frac{2\pi n_s n_p^2 r_{eff} E_D}{\lambda \cos\alpha} \frac{1}{1+\ell_s^2 K^2}. \tag{1}$$

Here $E_D = K(k_B T/e)$ is the diffusion field, K is the spatial frequency of the space-charge grating, T is the absolute temperature, k_B is the Boltzmann constant, e is the electron charge, r_{eff} is the effective Pockels coefficient, n_s and n_p are the refractive indices of the two interacting waves, λ is the light wavelength in vacuum, and α is the angle between the input face normal and wavevector of the signal wave. The Debye screening length, $\ell_s = [\varepsilon_{eff}\varepsilon_0 k_B T/(N_{eff} e^2)]^{1/2}$, depends on the effective trap density $N_{eff} = N_D N_T/(N_D + N_T)$, where N_D and N_T represent the densities of filled donors and empty traps, respectively; $\varepsilon_{eff}\varepsilon_0$ is the effective dielectric permittivity.

One problem of SPS, which is still not solved technologically, consists of an insufficient effective trap density that results in strong charge screening at high spatial frequencies, $\ell_s^2 K^2 \gg 1$ [1]. For interaction of counterpropagating waves this leads to considerable reduction of the gain factor because of large denominator of the second factor in Eq. (1), but at the same time allows for simplifying substantially the equation itself [4]

$$\Gamma = \frac{N_{eff} e}{2\varepsilon_0} \left(\frac{n^2 r_{eff}}{\varepsilon_{eff}} \right). \tag{2}$$

It is assumed in Eq. (2) that the coupling waves are exactly counterpropagating eigenwaves which have identical polarization such that $\mathbf{k}_s \| \mathbf{k}_p \| \mathbf{K}$, $n_s = n_p = n$ and $\mathbf{e}_s \cdot \mathbf{e}_p = 1$.

As follows from Eq. (2) the gain factor Γ is proportional to effective Pockels coefficient $r_{eff} = \hat{r}_{lmn} \mathbf{d}_l \mathbf{d}_m \mathbf{q}_n$ and is inversely proportional to effective dielectric constant $\varepsilon_{eff} = \hat{\varepsilon}_{ij} \mathbf{q}_i \mathbf{q}_j$. The dependences of the eigenwaves' unit electric displacement vector $\mathbf{d}$ and phase velocity $2\pi n/\lambda$ on unit wavevector $\mathbf{q} = \mathbf{K}/K$ should be also taken into account. When data on Pockels tensor $\hat{r}$, low-frequency dielectric tensor $\hat{\varepsilon}$, and optical indicatrix of the crystal are declared, the gain factor for each eigenwave depends only on its direction according to Eq. (2).

The publications on SPS characterization that provide the necessary information are not numerous: references [9–11] for low-frequency dielectric tensor; references [12, 13] for optical indicatrix; references [14–17] for Pockels tensor and two theses, [18] and [19]. The reported values are most often correct and reliable, however there is a difficulty in their use which is related either to imprecise description or description lacking at all of the Cartesian setting for

#217677 - $15.00 USD Received 23 Jul 2014; revised 22 Sep 2014; accepted 22 Sep 2014; published 2 Oct 2014

which the measurements have been done. Below we describe the choice of crystallophysic axes that we use in what follows and precise specifications of different anisotropic parameters of the crystal.

For polar phase of $Sn_2P_2S_6$ the elementary cell has the dimensions a = 9.375 Å, b = 7.488 Å, c = 6.513 Å and the angle between the axes a and c is β= 91.15°, while the two other angles are equal to 90° [20]. In the introduced crystallophysic orthogonal coordinate system (Fig. 1), the y-axis is set to be normal to the crystal mirror plane m, the z-axis coincides with the c-axis and the x-axis is aligned close to the a-axis. The question of crucial importance is the choice of positive directions of Cartesian axes; here we try to conform with the IEEE standard [21]. Following publication [22], the vector of the spontaneous polarization $\mathbf{P}_S$ is located between [100] and [101] crystallographic directions and therefore belongs to the quadrant I of the xz-plane. Referring to the study of piezoelectric properties of $Sn_2P_2S_6$ [23] it is accepted that both, the effective piezoelectric constant d_{eff} and effective dielectric permittivity ε_{eff} get their maximum values in the same quadrant of the xz-plane (so that d_{11} and d_{33} are both positive, in accordance with the standard requirement). The positive direction of the y-axis is then imposed by the right-hand rule convention for the x, y and z axes.

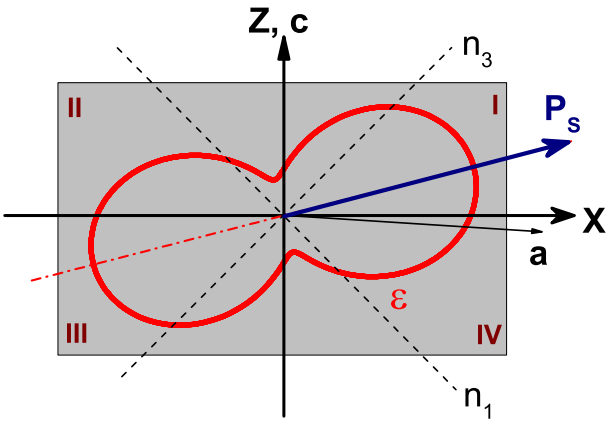

Fig. 1. The orientation of the crystallographic axes a and c, the spontaneous polarization vector $\mathbf{P_s}$, the major (n_3) and middle (n_1) axes of the optical indicatrix (dashed lines) of $Sn_2P_2S_6$ crystal in the crystallophysic coordinates. The angular dependence of the effective dielectric permittivity ε_{eff} is shown as a solid line. The quadrants are enumerated as I, II, III, and IV as it is shown in the corners of the gray area.

In the crystallophysic coordinate the Pockels tensor in contracted notation and the low-frequency dielectric tensor of $Sn_2P_2S_6$ read, respectively:

$$\frac{\hat{r}}{r_{11}} = \begin{pmatrix} 1 & 0 & -0.19 \\ 0.53 & 0 & -0.08 \\ 0.87 & 0 & -0.11 \\ 0 & -5\cdot 10^{-3} & 0 \\ -0.12 & 0 & 0.2 \\ 0 & -0.03 & 0 \end{pmatrix}, \tag{3}$$

#217677 - $15.00 USD Received 23 Jul 2014; revised 22 Sep 2014; accepted 22 Sep 2014; published 2 Oct 2014

$$\frac{\hat{\varepsilon}}{\varepsilon_{11}} = \begin{pmatrix} 1 & 0 & 0.2 \\ 0 & 0.1 & 0 \\ 0.2 & 0 & 0.25 \end{pmatrix}. \tag{4}$$

Taking the relative values in Eqs. (3) and (4) normalized to the largest component of each tensor doesn't affect the direction of the gain maximum that we are searching for, as it follows from Eq. (2).

The major axis of the optical indicatrix lies in quadrant I of the xz-plane and is tilted to $\varphi_0 = 43.3^\circ$ with respect to the x-axis [12]. The inverse optical-frequency dielectric tensor is represented in the form

$$\hat{B} = \begin{pmatrix} n_1^{-2}\sin^2\varphi_0 + n_3^{-2}\cos^2\varphi_0 & 0 & \frac{1}{2}(n_3^{-2} - n_1^{-2})\sin 2\varphi_0 \\ 0 & n_2^{-2} & 0 \\ \frac{1}{2}(n_3^{-2} - n_1^{-2})\sin 2\varphi_0 & 0 & n_1^{-2}\cos^2\varphi_0 + n_3^{-2}\sin^2\varphi_0 \end{pmatrix}, \tag{5}$$

where $n_1 = 3.0253$, $n_2 = 2.9309$, $n_3 = 3.0974$ are the principal refractive indexes of the SPS crystal at the wavelength $\lambda = 633$ nm [12]. The dependence of wave polarization $\mathbf{d}$ and refractive index n of each eigenwave on its direction $\mathbf{q}$ is obtained from wave equation $\mathbf{q} \times (\mathbf{q} \times \hat{B}\mathbf{d}) + \mathbf{d}n^{-2} = 0$. This equation is an example of an eigenvalue equation with matrix $M_{im} = \hat{e}_{ijk}\hat{e}_{klm}\mathbf{q}_j\mathbf{q}_l$, where $\hat{e}_{ijk}$ is Levi-Civita symbol. This is solved numerically using **dgeev** method of **LAPACK** library.

It is convenient to present the calculated dependences of the gain factor on spatial orientation of the grating vector $\mathbf{q}$ in spherical coordinates (see Fig. 2). The azimuth angle φ is measured from the x-axis in the counterclockwise direction, to be in agreement with the notation of quadrants in Fig. 1. The zenith angle θ is measured therefore from the negative direction of the y-axis.

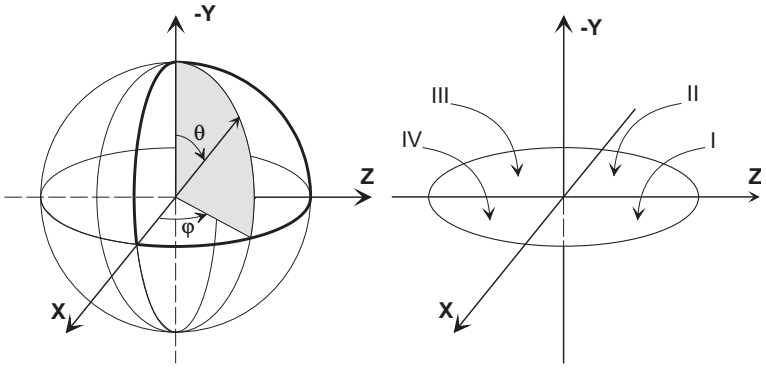

Fig. 2. Left drawing introduces spherical coordinates for orientation dependences of the gain factor. Right drawing shows the numeration of quadrants **I**, **II**, **III** and **IV** in the crystal mirror plane xz.

The results of calculation are shown in Fig. 3 for the fast eigenmode (which refers to the smaller refractive index, i.e., to inner shell of the normal surface) and slow eigenmode (which refers to the larger refractive index, i.e., to outer shell of the normal surface). The yellowish and bluish colors mark the positive and negative gain, respectively, while colorless regions indicate the areas of parameters with very small gain, approaching zero. The change to 180° of either φ or θ, which corresponds to rotation of the sample to 180° leads to inversion of the beam coupling direction (a change of the sign of Γ is represented in Fig. 3 by the change of color).

#217677 - $15.00 USD Received 23 Jul 2014; revised 22 Sep 2014; accepted 22 Sep 2014; published 2 Oct 2014

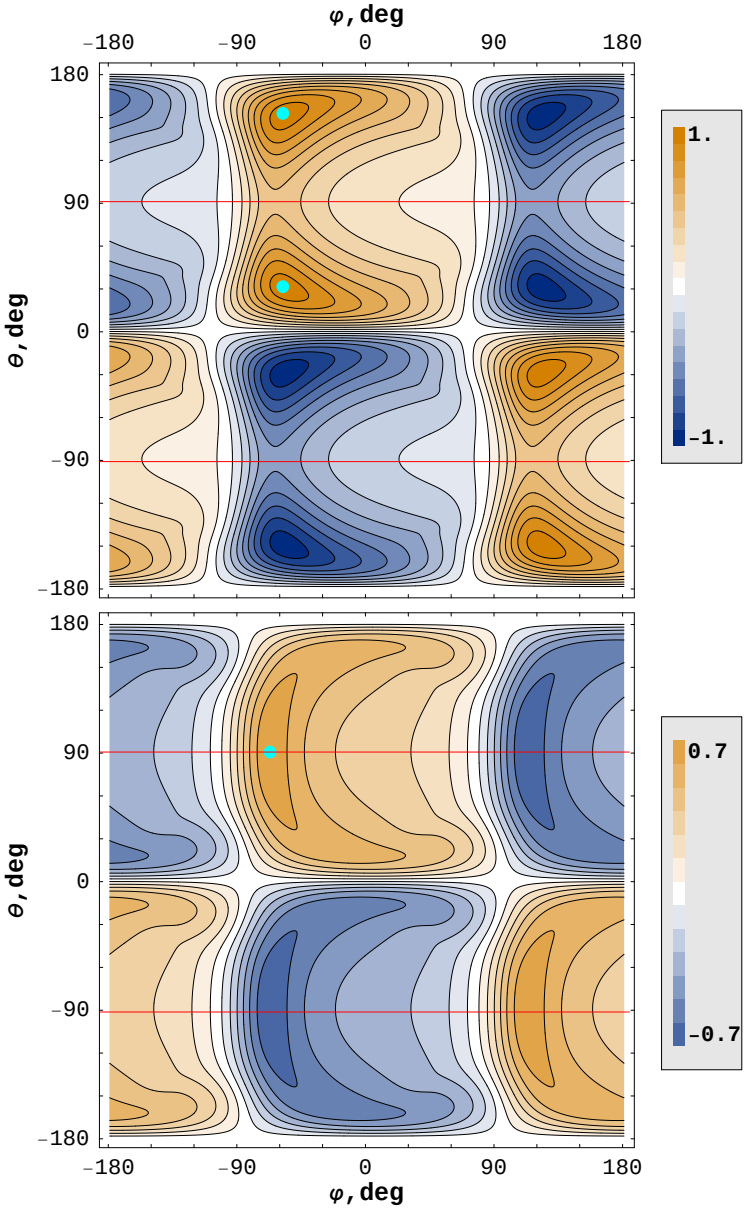

Fig. 3. Pseudocolor 2D maps that represent normalized two-beam coupling gain factor versus orientation of a pair of interacting counterpropagating crystal eigenwaves that belong to the inner and outer shells of the normal surface (upper and lower panels, respectively.) This calculation is done for light waves with 633 nm wavelength and $Sn_2P_2S_6$ crystal at ambient temperature. Red lines mark the crystal mirror plane *xz* while bright spots indicate signal wave orientation for which the largest gain factor can be achieved.

#217677 - $15.00 USD Received 23 Jul 2014; revised 22 Sep 2014; accepted 22 Sep 2014; published 2 Oct 2014

The *xz* coordinate plane corresponds to horizontal lines $\theta = \pm 90^\circ$. As the *xz* plane is a mirror plane of $Sn_2P_2S_6$ the values of gain factor calculated for any arbitrary φ remain the same if the zenith angle θ is changed to $(180^\circ - \theta)$. The two other crystallophysic planes, *xy* and *yz* correspond to vertical lines $\varphi = 0^\circ$, $\pm$ 180° and $\pm$ 90°, respectively. The largest gain factor that can be reached for the light waves that propagate in the *yz*-plane, as it follows from Fig. 3, is smaller than that for the waves propagating in the *xy*-plane. This is in agreement with the fact that the Pockels coefficients in the first column of Eq. (3) are larger than that of the third column.

The horizontal lines at $\theta = 0^\circ$ and $\pm$ 180° define the negative and positive directions of the *y*-axis. Because of absence of the nonvanishing *y*-components responsible for coupling of identically polarized light waves in the $Sn_2P_2S_6$ Pockels tensor ($r_{12} = r_{22} = r_{32} \equiv 0$), the gain factor for the waves that propagate along the *y*-axis is identically zero.

Finally, the main result of the calculation presented in Fig. 3 is in locating the wave directions with largest possible beam coupling. As one can see, for an eigenwave that corresponds to the inner shell of the normal surface the absolute maximum of Γ occurs at $\varphi \approx$ -57° and $\theta \approx$ 31° (or $\theta \approx 149^\circ$). At the same time, the optimum coupling direction for the eigenwave that corresponds to the outer shell is unique and appears in the mirror plane at $\varphi \approx$ -76°, $\theta = 90^\circ$. The bright blue spots show the positions of the positive gain maxima in Fig. 3.

These calculations allow for concluding that with the presently available $Sn_2P_2S_6$ crystals the optimum orientation of interacting waves is mainly determined by compromise between reducing of the charge screening and decreasing of effective Pockels coefficient, which occur when space charge field direction moves out of the *x*-axis towards the *y*- or *z*-axes.

As the first column components (r_{11}, r_{21}, r_{31}) are the largest among all Pockels tensor components of $Sn_2P_2S_6$, the maximum of the effective Pockels coefficient occurs at $\varphi \approx 0$. For the slow eigenmode, because of large r_{31}, the greatest effective Pockels coefficient is reached at $\theta \approx 90^\circ$. Therefore, the direction of largest gain factor for the slow eigenwave appears in the mirror plane and is located near the *z*-axis.

For small deviations from the mirror plane ($\theta \neq 90^\circ$), the fast eigenwaves are polarized nearly along the meridians. The direction that ensures the largest effective Pockels coefficient for this mode is out of the mirror plane ($\theta = 90^\circ$), because the contribution of the largest r_{11} component increases with (90°- θ); therefore, the direction of gain maximum for fast eigenwave is tilted in the *y*-direction too.

It should be noted that whatever the eigenwave is, the condition of the maximum gain is only weakly influenced by the components of the second and third columns of the Pockels tensor (Eq. (3)). The hierarchy of the Pockels tensor components defines, however, the ratio of the gain factor values at these maxima.

3. Experiment and discussion

The experimental measurements have been started with nominally undoped samples of $Sn_2P_2S_6$ cut along the crystallophysic axes [4]. With counterpropagating beams that enter the sample from the *x*-faces, we discovered that the normal incidence (grating vector **K** parallel to the *x*-axis) does not provide the largest two-beam coupling gain. This motivated calculations and further experimental efforts to find the optimum interaction geometry that could ensure the largest possible gain.

The use of the standard-cut samples of nominally undoped $Sn_2P_2S_6$ was, however, quite ineffective for the purpose of gain optimization because of two reasons. A quite high refraction of $Sn_2P_2S_6$ (all indices of refraction close to 3.0) strongly reduces the angular window in which a light wave can propagate inside the sample as Total Internal Reflection angle is less than 18°. Thus, the optimum directions of beam propagation shown by bright blue spots in 2D maps

#217677 - $15.00 USD Received 23 Jul 2014; revised 22 Sep 2014; accepted 22 Sep 2014; published 2 Oct 2014

of Fig. 3 are inaccessible from any sample face. A large index of refraction leads also to a considerable Fresnel reflection, which depends strongly on angle of incidence. This results in a considerable intensity variation of a light beam inside the sample when angle of incidence is changed. As the gain factor in $Sn_2P_2S_6$ is intensity dependent [1] the measured angular dependences of Γ become distorted.

To overcome these difficulties we (*i*) use the samples with special crystal cut that ensure the propagation along the optimum direction for a beam with a normal incidence to the input face, and (*ii*) select 1%Te-doped $Sn_2P_2S_6$ crystals [24] for measurements, as they have less pronounced intensity dependence of gain as compared to crystals with other known dopants and nominally undoped crystals.

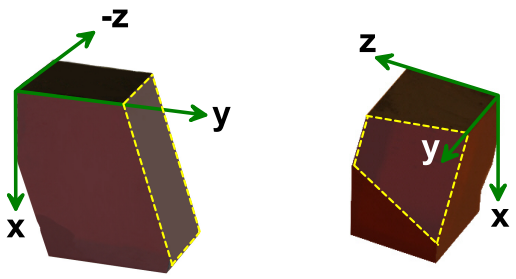

Fig. 4. The $Sn_2P_2S_6$ samples used in the experiment , #1 and #2, left and right, respectively. The arrows show the crystallophysic axes and the dashed line frames indicate the input faces.

Our first choice was to optimize the **K** direction in the *xy*-plane, for which the difference in dielectric tensor components is the largest possible ($\varepsilon_{11} \approx 10\varepsilon_{22}$, see Eq. (4)). This allowed for a reasonable expectation of a substantial inhibition of screening at an appropriately selected **K** direction. Based on the result of calculation presented in [4], the first sample (sample #1) was prepared with the input-output faces perpendicular to the *z*-axes and tilted to 20° with respect to the *xz*-plane (for the beam at normal incidence in the 2D maps of Fig. 3, the azimuth and zenith angles were φ = 0 and θ = 20°, respectively). The second sample (sample #2) had a more sophisticated cut, the normal to its input/output faces being aligned at φ = -60° and θ = 30°, which is close to the optimum direction that should maximize the gain factor for the fast eigenwave (see upper panel of Fig. 3). The outer appearance of these two samples is shown in Fig. 4, with arrows indicating the crystallophysic directions and yellow-dashed frames around the input faces. The thickness ℓ of the samples #1 (left) and #2 (right) in directions normal to the input/output faces is 8 mm and 4.4 mm, respectively.

Two unexpanded beams from a He-Ne laser (TEM_{00}, Gaussian beam waist $\approx$ 1.5 mm, λ = 633 nm, total power $\approx$ 30 mW) with the intensity ratio 1:200 were exactly counterpropagating to each other. The linear polarization of both beams was adjusted with half wave phase retarders to excite one of the crystal eigenwaves. The gain factor Γ was estimated with a standard expression

$$\Gamma = (1/\ell)\ln(I_s/I_{s0}), \tag{6}$$

where I_s and I_{s0} are the signal (weaker) beam intensity with and without the pump wave in the sample and ℓ is the interaction length inside the sample which is equal to the sample thickness in this case.

#217677 - $15.00 USD Received 23 Jul 2014; revised 22 Sep 2014; accepted 22 Sep 2014; published 2 Oct 2014

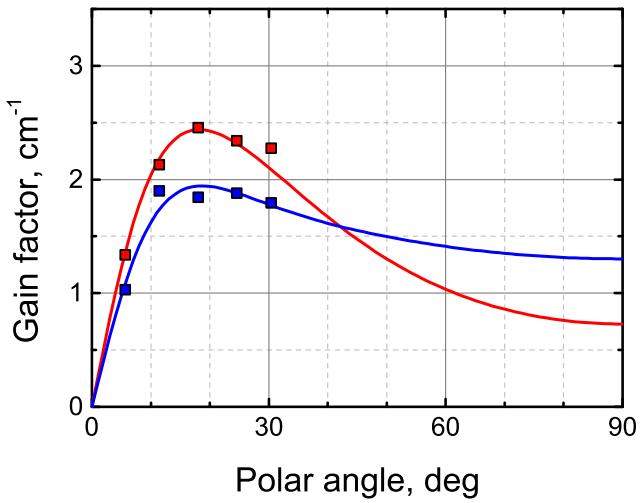

Fig. 5. Gain factor Γ versus tilt angle θ of grating vector **K** with respect to the *y*-axis in the *xy*-plane for azimuth angle $\varphi = 0$ (sample #1). Solid lines show the best fit with calculated dependences (see text). Red and blue colors mark the interaction of waves that belong to the inner and outer shells of the normal surface, respectively.

Figure 5 represents the angular dependence of the gain factor for two eigenwaves of sample #1. The sample was rotated so that the laser beams remained always in the *xy*-plane. The solid lines show the best fit of calculated dependences to the measured data, red (and blue) squares for inner (and outer) shells of the normal surface. Both curves feature quite distinct maxima slightly below θ = 20°. Note, that the largest gain is reached for the eigenwave which is only modestly enhanced for grating vector aligned along the the *x*-axis (θ = 90°, $\varphi = 0$).

At the same time, it is clearly seen from Fig. 6 that such an experimental geometry doesn't provide access to the predicted grating direction with maximal gain. Therefore we measure then, with the same sample #1, the angular dependence of the gain factor in the plane which is perpendicular to the *xy*-plane and perpendicular to the input/output faces. When tilting the incident beam in this plane we change both the azimuth angle φ and the zenith angle θ of the recorded grating vector **K** inside the sample so that grating vector moves in Fig. 6 along the trajectories shown by arcs.

The angular dependence of the gain factor for both eigenwaves measured with sample #1 in this geometry is shown on Fig. 7 as a function of azimuth φ. It is clearly seen that gain factor increases with the decreasing φ for both eigenwaves (red and blue open circles), in qualitative agreement with calculated data, shown by solid lines. Because of light refraction on the faces of sample #1 only part of predicted for this geometry grating orientations (shown by the solid lines on Fig. 6) is accessible and the largest value of gain factor cannot be reached with this sample.

To enter the convenient angular window we use the sample #2. The values of Γ measured with normal incidence to the input faces of these sample (φ = -60° , θ = 30°) are shown in Fig. 7 with red and blue squares. Taking into account that these data are measured with two different samples that may have different residual domain structure (different deviation from the ideal single domain state) the agreement of expected and measured gain enhancement for sample #2 is rather astonishing. Agreement of presented in Figs. 5 and 7 experimental and theoretical angular dependencies together with published before data [4] indirectly confirms the results of calculation shown in Fig. 3 and used set of material constants in Eqs. (3), (4) and (5).

#217677 - $15.00 USD Received 23 Jul 2014; revised 22 Sep 2014; accepted 22 Sep 2014; published 2 Oct 2014

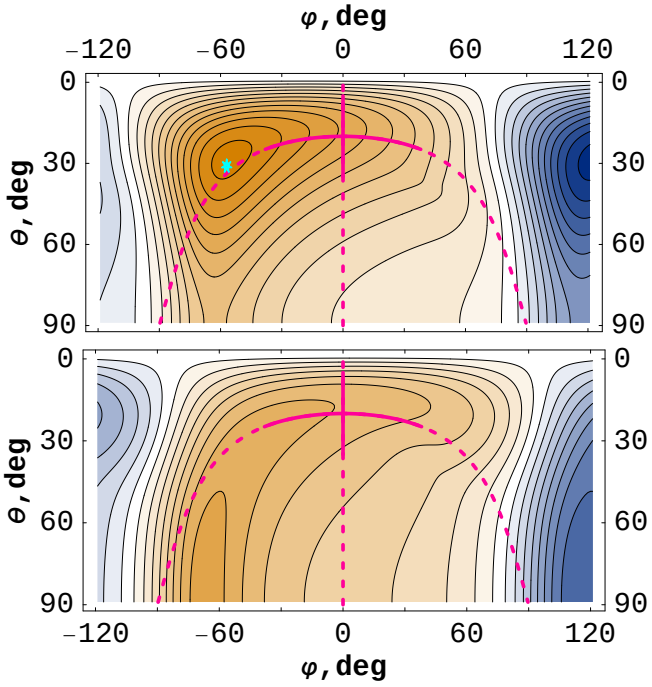

Fig. 6. A fragment of the 2D plot of gain factor angular dependence (Fig. 3) that represents actual positive gain aria. The red lines show how the grating vector direction changes in sample #1 when it is rotated above the *z*-axis (vertical lines), and above the axis tilted to 20° with respect to the *x*-axis in the *xy*-plane (arcs). The solid lines mark the angular windows inside the crystal that are accessible with sample #1, while the asterisk indicates the normal incidence to the input/output faces of the sample #2.

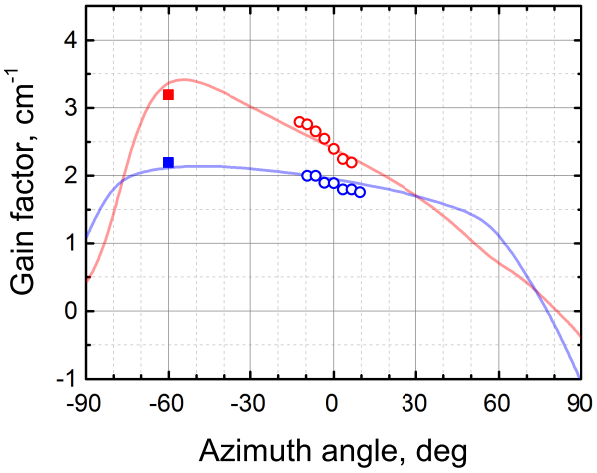

Fig. 7. Angular dependence of gain factor Γ measured with sample #1 (circles) and with sample #2 at normal incidence to the input face (squares). Solid lines show the best fit with calculated dependences (see text). Red and blue colors mark the interaction of waves that belong to the inner and outer shells of the normal surface, respectively.

#217677 - $15.00 USD Received 23 Jul 2014; revised 22 Sep 2014; accepted 22 Sep 2014; published 2 Oct 2014

4. Conclusions

The optimum geometry that maximizes the two-beam coupling gain for counterpropagating light beams in monoclinic photorefractive crystal is considered, with $Sn_2P_2S_6$ taken as an example. The optimum orientations of the two interacting waves are shown to be influenced mainly by the anisotropy of the dielectric and electrooptic properties. The best coupling of slow eigenwaves can be achieved within the crystal mirror plane. For fast eigenwaves the directions that ensure the largest gain are tilted symmetrically to the mirror plane; this is a consequence of the increasing effective electrooptic coefficient which incorporates, out of the mirror plane, the largest Pockels component r_{11} of $Sn_2P_2S_6$. The calculations performed with available data on optical and dielectric properties of $Sn_2P_2S_6$ show that in an optimized geometry the two-beam coupling gain for the fast eigenwaves can be 2.6 times increased as compared to previously considered classical orientation of waves along the crystal x-axis. This is confirmed experimentally with Te-doped $Sn_2P_2S_6$ crystal.

Appendix

In this Section the experimental techniques are described that are used for establishing the Cartesian set of axes with defined positive directions for our samples. Also, the test experiments are described that have been performed to confirm the orientation of major axes of the optical indicatrix and dielectric permittivity in the crystal mirror plane. These key directions are of crucial importance for correct calculation of spatial dependence of gain factor (see Sect. 2).

The first step in sample preparation for this study was in cutting a sufficiently large rectangular sample with faces normal to the crystallographic directions, which could be used further for preparing special cuts described above. This was done with the use of the X-ray diffraction analysis to control the axes orientation. The second step consisted in finding the positive axes directions for this crystal, which is lacking the symmetry center.

The positive direction of the x- and z-axes can be identified through the direction of the beam fanning from the beams that enter the sample via z-face or x-face, respectively. If photoexcited carriers are positively charged, which is the case for all presently known doped and nominally undoped $Sn_2P_2S_6$ crystals, the scattered light fan points in the positive (or negative) axis direction if positive (or negative) Pockels tensor component dominates in the effective Pockels coefficient. Thus the unidirectional light induced scattering (fanning) from the light beam that enters the sample through the z-face points to positive direction of the x-axis (whatever is its eigenpolarization, along the x-axis or the y-axis.) This is a consequence of positive signs of first column Pockels coefficients r_{11} and r_{21} (see Eq. (3)). Similarly, the beam that enters the sample through the x-face produces (less pronounced but still detectable) fanning in negative direction of the z-axis.

With the known positive directions of the x- and z-axes we can then check the orientation of the major axis of the optical indicatrix and identify the orientation of largest dielectric permittivity in the xz-plane. There are several possibilities to do this by profiting from various types of nonlinear wave mixing. The easiest way to find the eigenwave with a smaller index of refraction in the y-cut sample is via observation of conical parametric scattering as described in Ref. [25]. Typical ring-like scattering pattern (see Fig. 8) with the polarization orthogonal to the incident beam polarization can appear if and only if the incident beam belongs to the inner shell of the normal surface, i.e. with the incident beam that possesses the smaller index of refraction, n_1. Such a test confirmed our initial supposition that the longest axis of optical indicatrix (n_3) is located in the quadrant I of the xz-plane, as it is shown in Fig. 1. The other possible way to identify the orientation of optical indicatrix is in establishing conditions of observation of the anisotropic selfdiffraction, described for $Sn_2P_2S_6$ in Ref. [15]. This latter method may become preferable when working with thin or low-gain samples that do not feature detectable

#217677 - $15.00 USD Received 23 Jul 2014; revised 22 Sep 2014; accepted 22 Sep 2014; published 2 Oct 2014

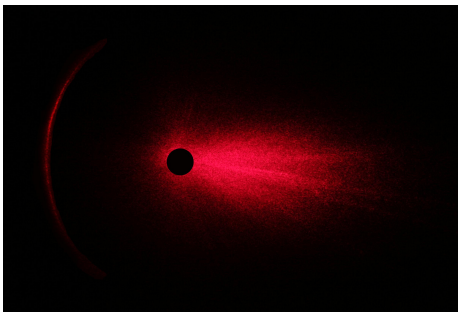

Fig. 8. Conical scattering pattern from a y-cut $Sn_2P_2S_6$ sample. The incident beam corresponds to the eigenwave of inner shell of the normal surface, while the light scattered into the bright arc on the left corresponds to the eigenwave of outer shell of the normal surface. The Polaroid sheet was placed behind the sample to filter out the transmitted light of the incident wave and reduce beam fanning.

parametric conical scattering.

Finally, we come to the identification of the orientation of the largest effective dielectric permittivity. In photorefractive materials the dielectric permittivity affects the dynamics of the recording/erasing process (via Maxwell relaxation time, $\tau_M = \varepsilon_{eff}\varepsilon_0/\sigma$, with σ being photoconductivity). If high enough, it also reduces the gain factor because of the space charge field screening, see Eq. (1). Thus, the necessary information on anisotropy of $\hat{\varepsilon}$ might be extracted from a measurement of the angular dependences of τ_M or Γ. We used the second option, measuring the gain factor for two co-propagating waves as a function of the sample rotation angle in the xz-plane (Fig. 9). When rotating the sample about the y-axis, the polarizations of the two recording waves were adjusted to belong to the same crystal eigenwave with the indices of refraction either n_1 or n_3 for upper and lower panels of Fig. 9, respectively.

The angle in air between two beams was adjusted to be 5° and 24° for the blue and red data in Fig. 9, respectively. The dependences of the gain factor in this geometry, for slow and fast eigenwaves, respectively, on rotation angle β have the form:

$$\Gamma \sim \frac{(r_{11} + r_{31} \pm 2r_{51})\cos\beta + (r_{13} + r_{33} \pm 2r_{53})\sin\beta}{1 + (2\pi\ell_{sX}/\Lambda)^2(\varepsilon_{11}\cos^2\beta + \varepsilon_{33}\sin^2\beta + \varepsilon_{13}\sin 2\beta)/\varepsilon_{11}}, \tag{7}$$

where ℓ_{sX} stands for Debye constant along the x-axis. In the first case (5°) charge screening is strongly reduced $(2\pi\ell_{sX}/\Lambda) \ll 1$ and the anisotropy of Pockels tensor plays a main role. In the second case (24°) charge screening is essential. Consequently, it was expected that the dielectric anisotropy should affect only the set of data shown in red, while data shown in blue should be insensitive to ε at all.

As one can see, the data measured with the small angle between the beams show an angular dependence with a detectable but rather small asymmetry with respect to the sign of the rotation angle. A much more pronounced asymmetry is clearly seen, on the contrary, for measurements with an increased angle between the beams. The maximum gain appears in the quadrant IV, which justifies the initial supposition that the largest value of ε falls into the quadrant I (see Fig. 1).

A satisfactory agreement of measured and calculated data justifies the choice of positive ε_{13} in the model. For comparison, we show with dashed lines the dependences calculated with the same absolute value of ε_{13}, but with the sign changed to be negative (maximum value of ε in the quadrant IV). The discrepancy with the measured data is obvious for such a choice of the ε anisotropy, thus supporting our conclusion that the largest ε appears in the quadrant I of the

#217677 - $15.00 USD Received 23 Jul 2014; revised 22 Sep 2014; accepted 22 Sep 2014; published 2 Oct 2014

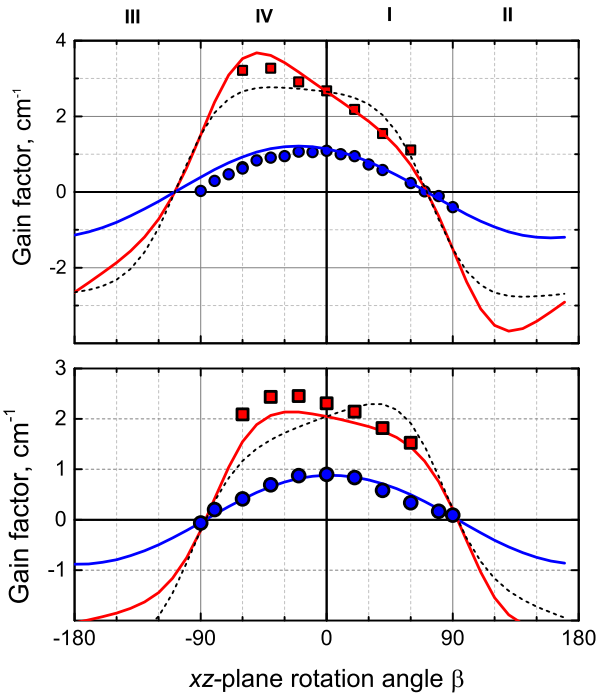

Fig. 9. Gain factor for coupling of two co-propagating waves versus orientation angle of the grating vector in the *xz*-plane. Circles and squares show the results of measurements for two different grating spacings, 7 μm and 1.5 μm, respectively. Both recording waves are polarized identically and belong to the outer shell (upper panel) and inner shell (lower panel) of the normal surface (index of refraction n_1 and n_3, respectively). The solid lines show fitting with Eq. (7) provided $2\pi\ell_{sX}$ =1.5 μm and ε_{13} is positive. The dashed line represents the calculation for hypothetic case, when the largest dielectric permittivity appears in the quadrant IV (i.e., when ε_{13} is negative.) The quadrants are numbered on top of the upper panel.

xz-plane as it is shown in Fig. 1.

Acknowledgments

The financial support of the European Office of Research and Development (EOARD) via Science and Technology Center of Ukraine (STCU Grants P585 and P438a) is gratefully acknowledged. We thank Professor Germano Montemezzani for valuable discussions.

#217677 - $15.00 USD Received 23 Jul 2014; revised 22 Sep 2014; accepted 22 Sep 2014; published 2 Oct 2014